

## Nodal-link semimetals

Zhongbo Yan,<sup>1</sup> Ren Bi,<sup>1</sup> Huitao Shen,<sup>2,1</sup> Ling Lu,<sup>3</sup> Shou-Cheng Zhang,<sup>4</sup> and Zhong Wang<sup>1,\*</sup>

<sup>1</sup>*Institute for Advanced Study, Tsinghua University, Beijing, 100084, China*

<sup>2</sup>*Department of physics, Massachusetts Institute of Technology, Cambridge, MA 02139, USA*

<sup>3</sup>*Institute of Physics, Chinese Academy of Sciences/Beijing National Laboratory for Condensed Matter Physics, Beijing 100190, China*

<sup>4</sup>*Department of Physics, Stanford University, CA 94305, USA*

In topological semimetals, the valence band and conduction band meet at zero-dimensional nodal points or one-dimensional nodal rings, which are protected by band topology and symmetries. In this Rapid Communication, we introduce “nodal-link semimetals”, which host linked nodal rings in the Brillouin zone. We put forward a general recipe based on the Hopf map for constructing models of nodal-link semimetal. The consequences of nodal ring linking in the Landau levels and Floquet properties are investigated.

Topological phases of matter have been among the most active research subjects in condensed matter physics. They can be broadly classified as two major classes. The first class of phases, including topological insulators and superconductors[1–6], and other symmetry protected topological phases[7], have gapped bulks with nontrivial topological structures characterized by topological invariants[8–15], dictating the existence of robust gapless modes on the boundary.

More recently, the second major class of topological materials, known as topological semimetals, have attracted widespread attentions. In the noninteracting limit, they are characterized by topologically robust  $\mathbf{k}$ -space band-touching manifolds, which can be zero-dimensional (0D) nodal points or one-dimensional (1D) nodal rings (or nodal lines). The bulk Dirac[16–25] and Weyl points[26–40] are responsible for novel phenomena related to chiral anomaly[41–51]. Moreover, bulk Weyl points entail surface Fermi arcs, while nodal rings[52–72] imply flat surface band (drumhead states) that may trigger interesting correlation effects[73]. Nodal rings have been predicted (e.g., Cu<sub>3</sub>PdN[60, 61], Hg<sub>3</sub>As<sub>2</sub>[74], Ca<sub>3</sub>P<sub>2</sub>[63, 75], 3D carbon networks[58], CaP<sub>3</sub>[76], Alkali Earth Metals[77, 78]) and experimentally studied in quite a few materials (e.g., PbTaSe<sub>2</sub>[62], ZrSiTe[79], ZrSiS[80–84]). Notably, nodal rings can be driven to Floquet Weyl points by circularly polarized light[85–89], accordingly, the drumhead surface states become Fermi arcs.

Unlike nodal points, nodal rings allow richer topological structures. They can touch at special points[60, 61, 90, 91], enabling formations of nodal chains[92, 93]. In this paper, we introduce new types of topological semimetals, dubbed “nodal-link semimetals”, which host nontrivially linked nodal rings[e.g., Fig.1(e)]. Furthermore, a method is introduced for constructing two-band models of nodal-link semimetals. We investigate generic physical consequences of nontrivial linking; in particular, a global toroidal  $\pi$  Berry phase generates a half-integer shift of Landau level index when the magnetic field is perpendicular to the ring plane. In addition, a suitable periodic external field can drive nodal-link semimetal to a Floquet Hopf insulator.

*Models.*—Nodal rings come from the crossing of two adjacent bands, thus we focus on two-band Bloch Hamiltonians,

which can generally be written as

$$H(\mathbf{k}) = a_0(\mathbf{k})\mathbf{1} + a_1(\mathbf{k})\tau_x + a_2(\mathbf{k})\tau_y + a_3(\mathbf{k})\tau_z, \quad (1)$$

where  $\mathbf{k} = (k_x, k_y, k_z)$ ,  $\tau_i$ 's are Pauli matrices, and  $a_0(\mathbf{k}) = 0$  will be adopted for simplicity (nonzero  $a_0$  can be trivially included, if needed). Nodal rings are protected by crystal symmetries. For concreteness, we take the  $PT$  symmetry[66, 94] that ensures the reality of  $H(\mathbf{k})$ , i.e.,  $a_2(\mathbf{k}) = 0$ . Now the spectra are  $E_{\pm}(\mathbf{k}) = \pm \sqrt{a_1^2 + a_3^2}$ , and the nodal rings are given by solving  $a_1(\mathbf{k}) = a_3(\mathbf{k}) = 0$ . A purpose of this paper is to construct models with mutually linked nodal rings.

Instead of taking trial-and-error approaches, we put forward a general method based on Hopf maps[95, 96]. They play special roles in quantum spin systems[95, 97], topological Hopf insulators[98–103], liquid-crystal solitons[104], quench dynamics of Chern insulators[105], and minimal models for topologically trivial superconductor-based Majorana zero modes[106]. Mathematically, a Hopf map is a nontrivial mapping from a 3-sphere  $S^3$  to a 2-sphere  $S^2$ , which possesses a nonzero Hopf invariant[95, 96, 98]. Moreover, it has the geometrical property that the preimage circles of any two points on  $S^2$  are linked. Mappings from a 3D torus  $T^3$  to  $S^2$  inherit the nontrivial topology of Hopf maps through  $T^3 \rightarrow S^3 \rightarrow S^2$ , where  $T^3 \rightarrow S^3$  is a map with unit winding number, and  $S^3 \rightarrow S^2$  is a Hopf map.

Given any vector function  $\mathbf{d}(\mathbf{k}) = (d_x, d_y, d_z)$  on the Brillouin zone  $T^3$ , one can define a mapping from  $T^3$  to  $S^2$  by  $\mathbf{k} \rightarrow \hat{\mathbf{d}}(\mathbf{k})$ , where  $\hat{\mathbf{d}} \equiv \mathbf{d}/|\mathbf{d}|$ . To define the Hopf invariant, it is convenient to express the vector  $\mathbf{d}$  in terms of a spinor, namely,  $d_i(\mathbf{k}) = z^\dagger \tau_i z$ , with  $z(\mathbf{k}) = (z_1, z_2)^T$ . Let us write  $z_1 = N_1 + iN_2, z_2 = N_3 + iN_4$ , then the Hopf invariant simplifies to[103]

$$n_h = \frac{1}{2\pi^2} \int d^3k \epsilon^{abcd} \hat{N}_a \partial_{k_x} \hat{N}_b \partial_{k_y} \hat{N}_c \partial_{k_z} \hat{N}_d, \quad (2)$$

where  $\hat{N}_a$  is the  $a$ -th component of the vector  $\mathbf{N} = (N_1, N_2, N_3, N_4)$  normalized to unit length.

Let us take a point on  $S^2$ , say  $\hat{\mathbf{n}}_1 = (0, 1, 0)$ . Under the mapping  $\mathbf{k} \rightarrow \hat{\mathbf{d}}(\mathbf{k})$ , all the preimages of  $\hat{\mathbf{n}}_1$  have to satisfy

$$d_x(\mathbf{k}) = d_z(\mathbf{k}) = 0, \quad (3)$$

however, the converse is not true, namely, a solution of Eq.(3) is not necessarily a preimage of  $\hat{\mathbf{n}}_1$ . In fact, the preimages

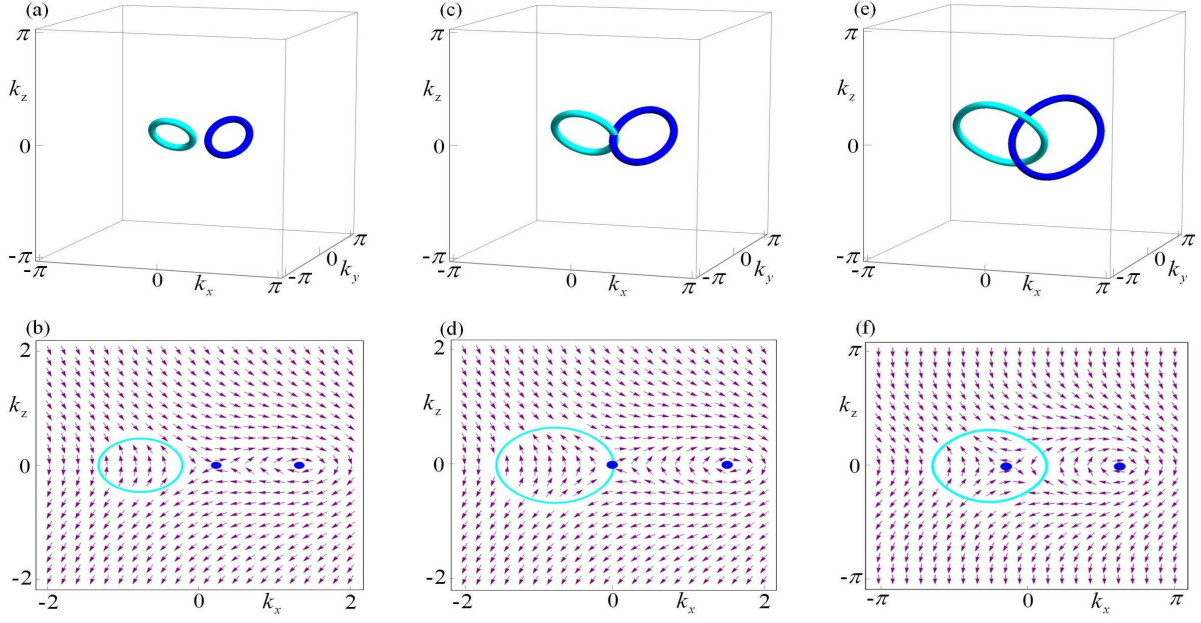


FIG. 1. Nodal rings of Eq.(6), and the pseudospin textures in the  $k_y = k_z$  plane, for (a,b)  $m_0 = 3.2$ , (c,d)  $m_0 = 3.0$ , and (e,f)  $m_0 = 2.5$ . The light blue ring locates in the  $k_y = k_z$  plane, while the dark blue ring is perpendicular to it.

of  $\hat{\mathbf{n}}_2 = (0, -1, 0)$  also satisfy Eq.(3). In a single equation, Eq.(3) gives the preimages of both  $\hat{\mathbf{n}}_1$  and  $\hat{\mathbf{n}}_2$ . This is among key observations in our construction. When  $n_h$  is nonzero, the preimages circles of any two points (say  $\hat{\mathbf{n}}_1$  and  $\hat{\mathbf{n}}_2$ ) are linked. Therefore, we can obtain linked nodal rings by taking

$$a_1(\mathbf{k}) = d_x(\mathbf{k}), \quad a_3(\mathbf{k}) = d_z(\mathbf{k}). \quad (4)$$

Recall that the  $a_2$  term is absent due to crystal symmetries, as discussed above. The same method also works if we start from a different  $\mathbf{n}_{1,2}$ ; for instance, taking  $\mathbf{n}_{1,2} = (0, 0, \pm 1)$  leads to  $a_1 = d_x, a_3 = d_y$ , which yields a nodal link as well.

This is a quite general approach to construct nodal-link semimetals. As an example, we take[98–103]

$$\begin{aligned} N_1 &= \sin k_x, \quad N_2 = \sin k_y, \quad N_3 = \sin k_z, \\ N_4 &= \cos k_x + \cos k_y + \cos k_z - m_0, \end{aligned} \quad (5)$$

which has  $n_h = -1$  for  $1 < m_0 < 3$  and  $n_h = 0$  for  $m_0 > 3$ . The explicit forms of  $d_i$ 's read

$$\begin{aligned} d_x &= 2 \sin k_x \sin k_z + 2 \sin k_y \left( \sum_{i=x,y,z} \cos k_i - m_0 \right), \\ d_y &= -2 \sin k_y \sin k_z + 2 \sin k_x \left( \sum_{i=x,y,z} \cos k_i - m_0 \right), \\ d_z &= \sin^2 k_x + \sin^2 k_y - \sin^2 k_z - \left( \sum_{i=x,y,z} \cos k_i - m_0 \right)^2. \end{aligned}$$

Following Eq.(4), a lattice model of nodal-link semimetal is

$$\begin{aligned} H(\mathbf{k}) &= [2 \sin k_x \sin k_z + 2 \sin k_y \left( \sum_{i=x,y,z} \cos k_i - m_0 \right)] \tau_x \\ &+ [\sin^2 k_x + \sin^2 k_y - \sin^2 k_z - \left( \sum_{i=x,y,z} \cos k_i - m_0 \right)^2] \tau_z. \end{aligned} \quad (6)$$

The nodal rings consist of points where both coefficients of  $\tau_x$  and  $\tau_z$  vanish. We find that one of the rings is  $k_y = k_z$ ,  $\sin k_x = m_0 - \sum_i \cos k_i$ , and the other is  $k_y = -k_z$ ,  $\sin k_x = \sum_i \cos k_i - m_0$ , shown in light and dark blue, respectively, in Fig.1. Fig.1(a) shows the unlinked rings for  $m_0 = 3.2$ , and Fig.1(e) illustrates the linked rings for  $m_0 = 2.5$  (a Hopf link). The critical point  $m_0 = 3.0$ , when the two rings cross each other, is shown in Fig.1(c). The direction of pseudospin vector ( $d_x, d_z$ ) is plotted in Fig.1(b)(d)(f), indicating that the light blue ring encloses a pseudospin vortex in the linked regime [Fig.1(f)], in contrast to the unlinked case [Fig.1(b)]. The surface states for  $m_0 = 2.5$  are shown in Fig.2. The two-disk-overlapping region has zero and two flat bands in Fig.2(a) and (c), respectively, which is consistent with the winding number[107] in each region.

Near the critical point[Fig.1(c)], we can expand the Hamiltonian as:

$$\begin{aligned} H(\mathbf{k}) &= [2k_x k_z + 2k_y(m - k^2/2)] \tau_x \\ &+ [k_x^2 + k_y^2 - k_z^2 - (m - k^2/2)^2] \tau_z, \end{aligned} \quad (7)$$

where  $k^2 = \sum_{i=x,y,z} k_i^2$ ,  $m = 3 - m_0$ . At the critical point  $m = 0$ , we have  $H(\mathbf{k}) \approx 2k_x k_z \tau_x + (k_x^2 + k_y^2 - k_z^2) \tau_z$ , thus the dispersion is quadratic in all three directions. Consequently, we find that, for  $m = 0$ , the density of states follows  $g(E) \sim \sqrt{E}$  near zero energy, in contrast to  $g(E) \sim E$  for  $m \neq 0$ . Just like that nontrivial topology of insulators can be undone by closing the energy gap, the nontrivial nodal-line linking can be untied through quadratic-dispersion critical points[Fig.1(c)], where  $g(E) \sim \sqrt{E}$ .

We remark that, although a nodal chain[92, 93] also contains crossings like Fig.1(c), its dispersion is not quadratic in all three directions at the crossing point, and the density of

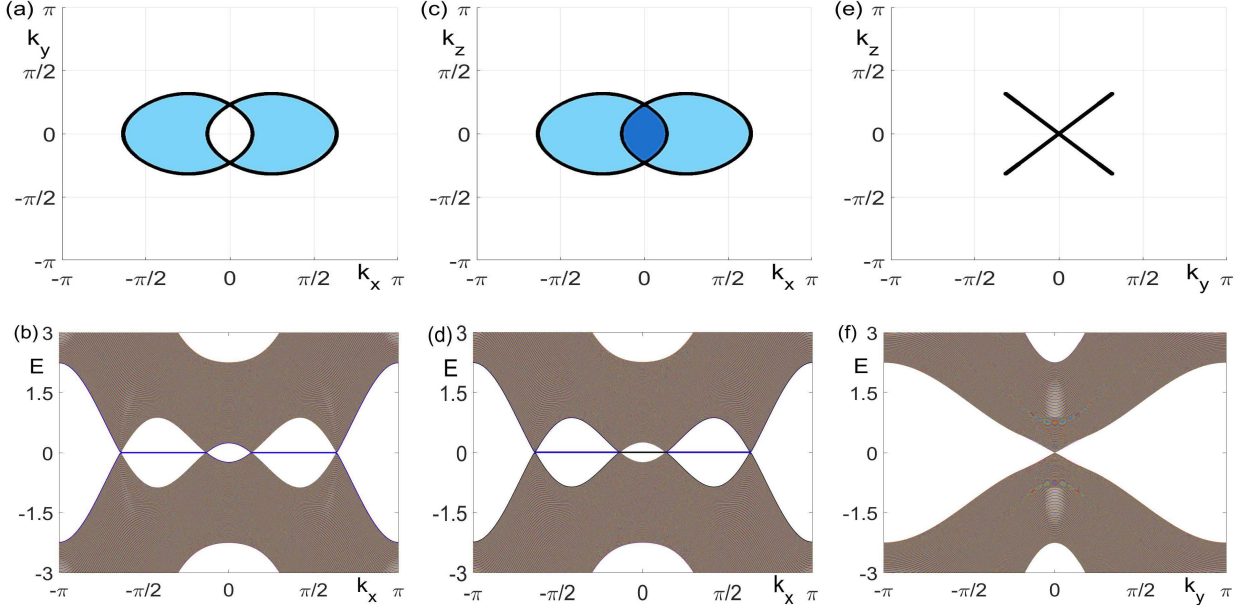


FIG. 2. (a) Surface flat bands for  $z = 0$  boundary. (b) The spectra as a function of  $k_x$  (fixed  $k_y = 0$ ) for a 800-site-thick slab perpendicular to  $z$  axis. (c) The  $y = 0$  surface states. (d) Spectra of a slab perpendicular to  $y$  axis. (e)  $x = 0$  surface Brillouin zone without surface states. (f) Spectra of a slab perpendicular to  $x$  axis. The black rings or lines in (a,c,e) are projections of the bulk nodal link to the surface Brillouin zone. In (c), the number of bands in the two-disk-overlapping region is twice that of the non-overlapping regions. Here,  $m_0 = 2.5$ .

states is linear instead of square-root.

*Landau levels.*—A key difference between a usual unlinked ring and a linked one is a global Berry phase along the ring. Let us draw a thin torus enclosing a nodal ring, then the Berry phase along the poloidal direction is always  $\pi$ ; in contrast, the Berry phase along the toroidal direction can be  $0$  or  $\pi$  (mod  $2\pi$ ), corresponding to the unlinked and linked ring, respectively [The  $0$  or  $\pi$  toroidal Berry phase of the light-blue ring can be read from the spin texture in Fig.1(b) and (f), respectively].

This  $\pi$  toroidal Berry phase can qualitatively affect the Landau levels. It is challenging to find analytic expressions of Landau levels for Eq.(6), nevertheless, a different model allows a simple solution: we take  $a_1 = d_x(\mathbf{k})$ ,  $a_3 = d_y(\mathbf{k})$  in Eq.(1). This Bloch Hamiltonian harbors four straight nodal lines at  $(k_x, k_y) = (0, 0)$ ,  $(0, \pi)$ ,  $(\pi, 0)$  and  $(\pi, \pi)$ , respectively. When  $1 < m_0 < 3$ , a nodal ring encircling  $(k_x, k_y) = (0, 0)$  is also found as  $\cos k_x + \cos k_y = m_0 - 1$  in the  $k_z = 0$  plane. Instead of working on this lattice Hamiltonian, we study its continuum limit for simplicity:

$$H(\mathbf{k}) = 2[k_x k_z + (m - Ck^2)k_y]\tau_x + 2[-k_y k_z + (m - Ck^2)k_x]\tau_y, \quad (8)$$

where  $k^2 = k_x^2 + k_y^2 + k_z^2$ .  $m = 3 - m_0$ , and  $C = 0.5$ . We have also done a basis change  $\tau_z \rightarrow \tau_y$  for later convenience. This model hosts a nodal line  $k_x = k_y = 0$  and a nodal ring  $k_x^2 + k_y^2 = m/C$  in the  $k_z = 0$  plane, which are linked.

Now we add a magnetic field along the  $z$  direction,  $\mathbf{B} = B\hat{z}$ . It is standard to do the replacement  $\mathbf{k} \rightarrow \mathbf{\Pi} = -i\nabla + e\mathbf{A}$  with  $\mathbf{A} = (0, Bx, 0)$ [108]. It is convenient to introduce the ladder operators,  $a = \frac{l_B}{\sqrt{2}}(\Pi_x - i\Pi_y)$ ,  $a^\dagger = \frac{l_B}{\sqrt{2}}(\Pi_x + i\Pi_y)$ , where  $l_B =$

$1/\sqrt{eB}$  is the magnetic length. The Hamiltonian becomes

$$H = \begin{pmatrix} 0 & f(k_z) \frac{\sqrt{2}a^\dagger}{l_B} \\ \frac{\sqrt{2}a}{l_B} f^\dagger(k_z) & 0 \end{pmatrix} \quad (9)$$

where  $f(k_z) = 2[k_z - i(m - Ck_z^2 - \frac{2Ca^\dagger a}{l_B^2})]$ . The Landau levels are found to be

$$E_{n,\pm}(k_z) = \begin{cases} \pm \sqrt{8n[k_z^2 + (m - Ck_z^2 - n\omega_c)^2]}/l_B, & n \geq 1, \\ 0, & n = 0, \end{cases} \quad (10)$$

where  $\omega_c \equiv 2C/l_B^2$ . The low energy eigenvalues are around  $n \sim 0$  and  $n \sim m/\omega_c$ , the former coming from the central nodal line at  $k_x = k_y = 0$ , while the latter coming from the nodal ring in the  $k_z = 0$  plane. As a comparison, we also consider a model with an unlinked ring:

$$H(\mathbf{k}) = (m - Ck^2)\tau_x + k_z\tau_z. \quad (11)$$

Following the same steps, we find that the Landau levels are

$$E_{n,\pm}(k_z) = \pm \sqrt{k_z^2 + [m - Ck_z^2 - (n + \frac{1}{2})\omega_c]^2}, n \geq 0. \quad (12)$$

Comparing Eq.(10) and Eq.(12), we see that the presence of a linked nodal line causes a shift of Landau level index by  $1/2$ , namely,  $n \rightarrow n - 1/2$ , which is a consequence of the  $\pi$  toroidal Berry phase. Such a shift can be measured by magneto-transport or magneto-optical experiments.

To highlight the effect of  $\pi$  Berry phase, we re-derive the Landau levels using semiclassical quantization[109–111]:

$$S(k_z) = 2\pi eB(n + 1/2 - \phi_B/2\pi), \quad (13)$$

where  $S$  is the cross-sectional area of a  $\mathbf{k}$ -space orbit, and  $\phi_B$  is the Berry phase along the orbit. For the linked ring, we have  $\phi_B = \pi$  (the toroidal Berry phase), and a semiclassical calculation (see Supplemental Material for details) yields the Landau levels in Eq.(10).

*Floquet Hopf insulator from nodal link.*—We will show that driving the nodal-link semimetal described by Eq.(8) creates a Floquet Hopf insulator. We consider a periodic driving generated by a circularly polarized light(CPL) propagating in  $z$  direction. The vector potential  $\mathbf{A}(t) = A_0(\cos \omega t, \eta \sin \omega t, 0)$ , where  $\eta = 1$  and  $-1$  stands for right-handed and left-handed CPL, respectively. Its effect is described by the minimal coupling,  $H(\mathbf{k}) \rightarrow H[\mathbf{k} + e\mathbf{A}(t)]$ . The full Hamiltonian is time-periodic,  $H(\mathbf{k}, t + T) = H(\mathbf{k}, t)$  with  $T = 2\pi/\omega$ , thus, it can be expanded as  $H(\mathbf{k}, t) = \sum_n \mathcal{H}_n(\mathbf{k})e^{in\omega t}$ , with

$$\begin{aligned} \mathcal{H}_0(\mathbf{k}) &= 2[k_x k_z + k_y(\tilde{m}_2 - Ck^2)]\tau_x \\ &\quad + 2[-k_y k_z + k_x(\tilde{m}_2 - Ck^2)]\tau_y, \\ \mathcal{H}_{\pm 1}(\mathbf{k}) &= eA_0[k_z \mp i\eta(\tilde{m}_1 - Ck^2) - 2Ck_y(k_x \mp i\eta k_y)]\tau_x \\ &\quad + eA_0[\pm i\eta k_z + (\tilde{m}_1 - Ck^2) - 2Ck_x(k_x \mp i\eta k_y)]\tau_y, \\ \mathcal{H}_{\pm 2}(\mathbf{k}) &= Ce^2 A_0^2 [(k_y \pm i\eta k_x)\tau_x - (k_x \mp i\eta k_y)\tau_y], \end{aligned} \quad (14)$$

where  $\tilde{m}_{j=1,2} = m - jCe^2 A_0^2$ . In the off-resonance regime, we can use an effective time-independent Hamiltonian[112–120]:

$$\begin{aligned} H_{\text{eff}}(\mathbf{k}) &= \mathcal{H}_0 + \sum_{n \geq 1} \frac{[\mathcal{H}_n, \mathcal{H}_{-n}]}{n\omega} + O\left(\frac{1}{\omega^2}\right) \\ &= 2[k_x k_z + k_y(\tilde{m}_2 - Ck^2)]\tau_x + 2[-k_y k_z + k_x(\tilde{m}_2 - Ck^2)]\tau_y \\ &\quad + \lambda[k_z^2 + (\tilde{m}_1 - Ck^2)^2 - 2Ck_p^2(\tilde{m}_1 - Ck^2 - \frac{\gamma}{4})]\tau_z, \end{aligned} \quad (15)$$

where  $\lambda = 4\eta e^2 A_0^2/\omega$ ,  $\gamma = Ce^2 A_0^2$ , and  $k_p = \sqrt{k_x^2 + k_y^2}$ . The energy spectrum of  $H_{\text{eff}}$  is fully gapped. For weak driving, the minima of the band are located at  $k_z = 0$ ,  $Ck_p^2 = \tilde{m}_2$ , and the gap is estimated as  $E_g \approx 12mC(eA_0)^4/\omega$ . In the CPL approach, this gap is expected to be rather small. It can be promoted to the order of  $(eA_0)^2$  by adding a small  $\Delta\tau_z$  pseudo-Zeeman term (see Supplemental Material for details of calculation).

If we remove the  $\tau_z$  term, Eq.(15) hosts a nodal ring and a nodal line linked together. It is readily checked that the coefficient of  $\tau_z$  is positive on the line and negative on the ring (for  $\eta = +1$ ), thus, the corresponding unit  $\hat{\mathbf{d}}$  vector is  $(0, 0, 1)$  and  $(0, 0, -1)$ , respectively. This fact suggests that Eq.(15) describes a (Floquet) Hopf insulators[98–103], or more precisely, a Floquet Hopf-Chern insulator[102], because the Chern number  $C(k_z) = -2$  for arbitrary  $k_z$ , as found in our numerical calculation. In the definition of Hopf invariant[95, 98], a nonsingular global Berry potential is needed, which is impossible in the presence of nonzero Chern number, nevertheless, we can study topological surface states. For a slab perpendicular to the  $z$  direction, we can solve the differential equation  $H_{\text{eff}}(k_x, k_y, -i\partial_z)\Psi_{k_x, k_y}(z) = E(k_x, k_y)\Psi_{k_x, k_y}(z)$ , which gives one surface band for each surface, whose dispersion is (see Supplemental Material for calculation):  $E_\alpha(\mathbf{k}) = \alpha\lambda[\tilde{m}_2/C + \gamma^2 - (1 + 3C\gamma/2)k_p^2]$ , where

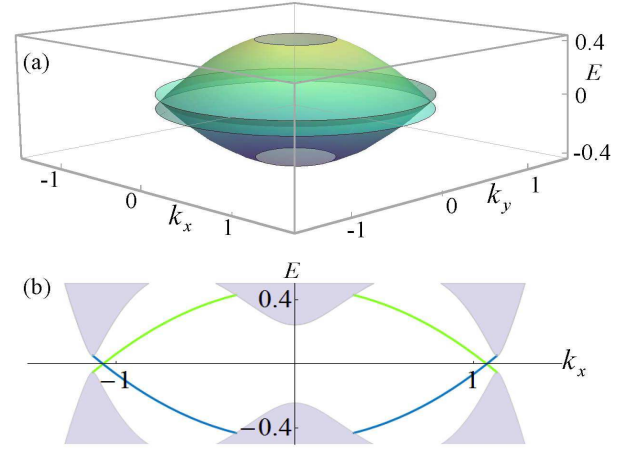


FIG. 3. Surface states of a slab perpendicular to the  $z$  axis. Parameters are  $\omega = 4$ ,  $m = 1$ ,  $eA_0 = 0.6$ ,  $C = 0.5$ . (a) 3D view of surface bands. (b)  $E(k_x)$  with  $k_y = 0$  fixed. The grey regions are bulk bands.

$\alpha = + (-)$  for top (bottom) surface. Shown in Fig.3, this dispersion is characteristic of a Hopf insulator[98]. For a fixed  $\theta$  (defined as  $\theta = \arctan k_y/k_x$ ), the surface state of either top or bottom surface is chiral, which can be understood in terms of a Chern number in the  $(k_\rho, k_z)$  space[103].

*Conclusions.*—We have introduced nodal-link semimetals into the family of topological semimetals. A general method for their model construction has been put forward. These phases may be realized by tuning the hoppings in optical lattices. Finding a solid-state material will be an important progress. It will also be worthwhile to study possible novel effects of linking. Theoretically, our models lay useful ground work for topological field theories[121] in the Brillouin zone.

*Note added.*—After finishing this manuscript, we became aware of a related eprint by Chen et al[122], in which a double-helix link is constructed without using the Hopf map. In another recent work, the Hopf map method has been generalized by Ezawa to construct other nodal links[123].

*Acknowledgements.*—We thank Chen Fang for useful comment. Z.Y., R.B., and Z.W. are supported by NSFC (No. 11674189). Z.Y. is supported in part by China Postdoctoral Science Foundation (2016M590082). L.L is supported by the Ministry of Science and Technology of China (No. 2016YFA0302400) and the National Thousand-Young-Talents Program of China. S.C.Z. is supported by NSF (No. DMR-1305677).

\* wangzhongemail@tsinghua.edu.cn

- [1] M. Z. Hasan and C. L. Kane, “Colloquium : Topological insulators,” Rev. Mod. Phys. **82**, 3045–3067 (2010).
- [2] Xiao-Liang Qi and Shou-Cheng Zhang, “Topological insulators and superconductors,” Rev. Mod. Phys. **83**, 1057–1110 (2011).
- [3] Ching-Kai Chiu, Jeffrey C. Y. Teo, Andreas P. Schnyder, and

- Shinsei Ryu, "Classification of topological quantum matter with symmetries," *Rev. Mod. Phys.* **88**, 035005 (2016).
- [4] A. Bansil, Hsin Lin, and Tanmoy Das, "Colloquium : Topological band theory," *Rev. Mod. Phys.* **88**, 021004 (2016).
- [5] B Andrei Bernevig and Taylor L Hughes, *Topological insulators and topological superconductors* (Princeton University Press, 2013).
- [6] Shun-Qing Shen, *Topological Insulators: Dirac Equation in Condensed Matters*, Vol. 174 (Springer Science & Business Media, 2013).
- [7] Xie Chen, Zheng-Cheng Gu, Zheng-Xin Liu, and Xiao-Gang Wen, "Symmetry protected topological orders and the group cohomology of their symmetry group," *Physical Review B* **87**, 155114 (2013).
- [8] D. J. Thouless, M. Kohmoto, M. P. Nightingale, and M. den Nijs, "Quantized hall conductance in a two-dimensional periodic potential," *Phys. Rev. Lett.* **49**, 405–408 (1982).
- [9] Qian Niu, D. J. Thouless, and Yong-Shi Wu, "Quantized hall conductance as a topological invariant," *Phys. Rev. B* **31**, 3372–3377 (1985).
- [10] C. L. Kane and E. J. Mele, " $Z_2$  topological order and the quantum spin Hall effect," *Phys. Rev. Lett.* **95**, 146802 (2005).
- [11] Liang Fu, C. L. Kane, and E. J. Mele, "Topological insulators in three dimensions," *Phys. Rev. Lett.* **98**, 106803 (2007).
- [12] J. E. Moore and L. Balents, "Topological invariants of time-reversal-invariant band structures," *Phys. Rev. B* **75**, 121306 (2007).
- [13] Xiao-Liang Qi, Taylor Hughes, and Shou-Cheng Zhang, "Topological Field Theory of Time-Reversal Invariant Insulators," *Phys. Rev. B* **78**, 195424 (2008).
- [14] Andreas P. Schnyder, Shinsei Ryu, Akira Furusaki, and Andreas W. W. Ludwig, "Classification of topological insulators and superconductors in three spatial dimensions," *Phys. Rev. B* **78**, 195125 (2008).
- [15] Zhong Wang and Shou-Cheng Zhang, "Simplified topological invariants for interacting insulators," *Phys. Rev. X* **2**, 031008 (2012).
- [16] ZK Liu, B Zhou, Y Zhang, ZJ Wang, HM Weng, D Prabhakaran, S-K Mo, ZX Shen, Z Fang, X Dai, *et al.*, "Discovery of a three-dimensional topological dirac semimetal, na<sub>3</sub>bi," *Science* **343**, 864–867 (2014).
- [17] M. Neupane, S.-Y. Xu, R. Sankar, N. Alidoust, G. Bian, C. Liu, I. Belopolski, T.-R. Chang, H.-T. Jeng, H. Lin, A. Bansil, F. Chou, and M. Z. Hasan, "Observation of a three-dimensional topological Dirac semimetal phase in high-mobility Cd<sub>3</sub>As<sub>2</sub>," *Nature Communications* **5**, 3786 (2014), arXiv:1309.7892 [cond-mat.mes-hall].
- [18] Sergey Borisenko, Quinn Gibson, Danil Evtushinsky, Volodymyr Zabolotnyy, Bernd Büchner, and Robert J. Cava, "Experimental realization of a three-dimensional dirac semimetal," *Phys. Rev. Lett.* **113**, 027603 (2014).
- [19] Su-Yang Xu, Chang Liu, Satya K Kushwaha, Raman Sankar, Jason W Krizan, Ilya Belopolski, Madhab Neupane, Guang Bian, Nasser Alidoust, Tay-Rong Chang, *et al.*, "Observation of fermi arc surface states in a topological metal," *Science* **347**, 294–298 (2015).
- [20] Steve M Young, Saad Zaheer, Jeffrey CY Teo, Charles L Kane, Eugene J Mele, and Andrew M Rappe, "Dirac semimetal in three dimensions," *Physical review letters* **108**, 140405 (2012).
- [21] Zhijun Wang, Yan Sun, Xing-Qiu Chen, Cesare Franchini, Gang Xu, Hongming Weng, Xi Dai, and Zhong Fang, "Dirac semimetal and topological phase transitions in a 3 bi (a= na, k, rb)," *Physical Review B* **85**, 195320 (2012).
- [22] Zhijun Wang, Hongming Weng, Quansheng Wu, Xi Dai, and Zhong Fang, "Three-dimensional dirac semimetal and quantum transport in cd 3 as 2," *Physical Review B* **88**, 125427 (2013).
- [23] C. Zhang, E. Zhang, Y. Liu, Z.-G. Chen, S. Liang, J. Cao, X. Yuan, L. Tang, Q. Li, T. Gu, Y. Wu, J. Zou, and F. Xiu, "Detection of chiral anomaly and valley transport in Dirac semimetals," *ArXiv e-prints* (2015), arXiv:1504.07698 [cond-mat.mtrl-sci].
- [24] R. Y. Chen, Z. G. Chen, X.-Y. Song, J. A. Schneeloch, G. D. Gu, F. Wang, and N. L. Wang, "Magnetoinfrared spectroscopy of landau levels and zeeman splitting of three-dimensional massless dirac fermions in zrte<sub>5</sub>," *Phys. Rev. Lett.* **115**, 176404 (2015).
- [25] Yanwen Liu, Xiang Yuan, Cheng Zhang, Zhao Jin, Awadhesh Narayan, Chen Luo, Zhigang Chen, Lei Yang, Jin Zou, Xing Wu, *et al.*, "Zeeman splitting and dynamical mass generation in dirac semimetal zrte<sub>5</sub>," *Nature communications* **7**, 12516 (2016).
- [26] Xiangang Wan, Ari M. Turner, Ashvin Vishwanath, and Sergey Y. Savrasov, "Topological semimetal and fermi-arc surface states in the electronic structure of pyrochlore iridates," *Phys. Rev. B* **83**, 205101 (2011).
- [27] G. E. Volovik, *The Universe in a Helium Droplet* (Oxford University Press, USA, 2003).
- [28] Kai-Yu Yang, Yuan-Ming Lu, and Ying Ran, "Quantum hall effects in a weyl semimetal: Possible application in pyrochlore iridates," *Phys. Rev. B* **84**, 075129 (2011).
- [29] A. A. Burkov and Leon Balents, "Weyl semimetal in a topological insulator multilayer," *Phys. Rev. Lett.* **107**, 127205 (2011).
- [30] Hongming Weng, Chen Fang, Zhong Fang, B. Andrei Bernevig, and Xi Dai, "Weyl semimetal phase in noncentrosymmetric transition-metal monophosphides," *Phys. Rev. X* **5**, 011029 (2015).
- [31] S.-M. Huang, S.-Y. Xu, I. Belopolski, C.-C. Lee, G. Chang, B. Wang, N. Alidoust, G. Bian, M. Neupane, A. Bansil, H. Lin, and M. Zahid Hasan, "An inversion breaking Weyl semimetal state in the TaAs material class," *Nature Communications* **6**, 7373 (2015).
- [32] Su-Yang Xu, Ilya Belopolski, Nasser Alidoust, Madhab Neupane, Guang Bian, Chenglong Zhang, Raman Sankar, Guoqing Chang, Zhujun Yuan, Chi-Cheng Lee, *et al.*, "Discovery of a weyl fermion semimetal and topological fermi arcs," *Science* **349**, 613–617 (2015).
- [33] BQ Lv, HM Weng, BB Fu, XP Wang, H Miao, J Ma, P Richard, XC Huang, LX Zhao, GF Chen, *et al.*, "Experimental discovery of weyl semimetal taas," *Physical Review X* **5**, 031013 (2015).
- [34] LX Yang, ZK Liu, Yan Sun, Han Peng, HF Yang, Teng Zhang, Bo Zhou, Yi Zhang, YF Guo, Marein Rahn, *et al.*, "Weyl semimetal phase in the non-centrosymmetric compound taas," *Nature physics* **11**, 728–732 (2015).
- [35] Xiaochun Huang, Lingxiao Zhao, Yujia Long, Peipei Wang, Dong Chen, Zhanhai Yang, Hui Liang, Mianqi Xue, Hongming Weng, Zhong Fang, Xi Dai, and Genfu Chen, "Observation of the chiral-anomaly-induced negative magnetoresistance in 3d weyl semimetal taas," *Phys. Rev. X* **5**, 031023 (2015).
- [36] S.-Y. Xu, N. Alidoust, I. Belopolski, C. Zhang, G. Bian, T.-R. Chang, H. Zheng, V. Stokov, D. S. Sanchez, G. Chang, Z. Yuan, D. Mou, Y. Wu, L. Huang, C.-C. Lee, S.-M. Huang, B. Wang, A. Bansil, H.-T. Jeng, T. Neupert, A. Kaminski, H. Lin, S. Jia, and M. Zahid Hasan, "Discovery of Weyl semimetal NbAs," *ArXiv e-prints* (2015),

- arXiv:1504.01350 [cond-mat.mes-hall].
- [37] Chandra Shekhar, Ajaya K Nayak, Yan Sun, Marcus Schmidt, Michael Nicklas, Inge Leermakers, Uli Zeitler, Yuri Skourski, Jochen Wosnitzer, Zhongkai Liu, *et al.*, “Extremely large magnetoresistance and ultrahigh mobility in the topological weyl semimetal candidate nbp,” *Nature Physics* **11**, 645–649 (2015).
- [38] Ling Lu, Liang Fu, John D Joannopoulos, and Marin Soljačić, “Weyl points and line nodes in gyroid photonic crystals,” *Nature photonics* **7**, 294–299 (2013).
- [39] Ling Lu, Zhiyu Wang, Dexin Ye, Lixin Ran, Liang Fu, John D. Joannopoulos, and Marin Soljačić, “Experimental observation of weyl points,” **349**, 622–624 (2015).
- [40] Alexey A Soluyanov, Dominik Gresch, Zhijun Wang, Quan-Sheng Wu, Matthias Troyer, Xi Dai, and B Andrei Bernevig, “Type-II Weyl semimetals,” *Nature* **527**, 495–498 (2015).
- [41] D. T. Son and B. Z. Spivak, “Chiral Anomaly and Classical Negative Magnetoresistance of Weyl Metals,” ArXiv e-prints (2012), arXiv:1206.1627 [cond-mat.mes-hall].
- [42] Chao-Xing Liu, Peng Ye, and Xiao-Liang Qi, “Chiral gauge field and axial anomaly in a weyl semimetal,” *Phys. Rev. B* **87**, 235306 (2013).
- [43] Vivek Aji, “Adler-bell-jackiw anomaly in weyl semimetals: Application to pyrochlore iridates,” *Phys. Rev. B* **85**, 241101 (2012).
- [44] A. A. Zyuzin and A. A. Burkov, “Topological response in Weyl semimetals and the chiral anomaly,” ArXiv e-prints (2012), arXiv:1206.1868 [cond-mat.mes-hall].
- [45] Zhong Wang and Shou-Cheng Zhang, “Chiral anomaly, charge density waves, and axion strings from weyl semimetals,” *Phys. Rev. B* **87**, 161107 (2013).
- [46] P. Hosur and X. Qi, “Recent developments in transport phenomena in Weyl semimetals,” *Comptes Rendus Physique* **14**, 857–870 (2013), arXiv:1309.4464 [cond-mat.str-el].
- [47] Pavan Hosur and Xiao-Liang Qi, “Tunable circular dichroism due to the chiral anomaly in weyl semimetals,” *Phys. Rev. B* **91**, 081106 (2015).
- [48] Heon-Jung Kim, Ki-Seok Kim, J.-F. Wang, M. Sasaki, N. Satoh, A. Ohnishi, M. Kitaura, M. Yang, and L. Li, “Dirac versus weyl fermions in topological insulators: Adler-bell-jackiw anomaly in transport phenomena,” *Phys. Rev. Lett.* **111**, 246603 (2013).
- [49] S. A. Parameswaran, T. Grover, D. A. Abanin, D. A. Pesin, and A. Vishwanath, “Probing the chiral anomaly with non-local transport in three-dimensional topological semimetals,” *Phys. Rev. X* **4**, 031035 (2014).
- [50] Q. Li, D. E. Kharzeev, C. Zhang, Y. Huang, I. Pletikosić, A. V. Fedorov, R. D. Zhong, J. A. Schneeloch, G. D. Gu, and T. Valla, “Chiral magnetic effect in  $ZrTe_5$ ,” *Nature Physics* **12**, 550–554 (2016), arXiv:1412.6543 [cond-mat.str-el].
- [51] Ren Bi and Zhong Wang, “Unidirectional transport in electronic and photonic weyl materials by dirac mass engineering,” *Phys. Rev. B* **92**, 241109 (2015).
- [52] A. A. Burkov, M. D. Hook, and Leon Balents, “Topological nodal semimetals,” *Phys. Rev. B* **84**, 235126 (2011).
- [53] Jean-Michel Carter, V. Vijay Shankar, M. Ahsan Zeb, and Hae-Young Kee, “Semimetal and topological insulator in perovskite iridates,” *Phys. Rev. B* **85**, 115105 (2012).
- [54] Michael Phillips and Vivek Aji, “Tunable line node semimetals,” *Phys. Rev. B* **90**, 115111 (2014).
- [55] M. Zeng, C. Fang, G. Chang, Y.-A. Chen, T. Hsieh, A. Bansil, H. Lin, and L. Fu, “Topological semimetals and topological insulators in rare earth mononictides,” ArXiv e-prints (2015), arXiv:1504.03492 [cond-mat.mes-hall].
- [56] Yige Chen, Yuan-Ming Lu, and Hae-Young Kee, “Topological crystalline metal in orthorhombic perovskite iridates,” *Nature communications* **6**, 6593 (2015).
- [57] Ching-Kai Chiu and Andreas P. Schnyder, “Classification of reflection-symmetry-protected topological semimetals and nodal superconductors,” *Phys. Rev. B* **90**, 205136 (2014).
- [58] Hongming Weng, Yunye Liang, Qianan Xu, Rui Yu, Zhong Fang, Xi Dai, and Yoshiyuki Kawazoe, “Topological nodal-line semimetal in three-dimensional graphene networks,” *Phys. Rev. B* **92**, 045108 (2015).
- [59] Kieran Mullen, Bruno Uchoa, and Daniel T. Glatzhofer, “Line of dirac nodes in hyperhoneycomb lattices,” *Phys. Rev. Lett.* **115**, 026403 (2015).
- [60] Rui Yu, Hongming Weng, Zhong Fang, Xi Dai, and Xiao Hu, “Topological node-line semimetal and dirac semimetal state in antiperovskite  $Cu_3PdN$ ,” *Phys. Rev. Lett.* **115**, 036807 (2015).
- [61] Youngkuk Kim, Benjamin J. Wieder, C. L. Kane, and Andrew M. Rappe, “Dirac line nodes in inversion-symmetric crystals,” *Phys. Rev. Lett.* **115**, 036806 (2015).
- [62] G. Bian, T.-R. Chang, R. Sankar, S.-Y. Xu, H. Zheng, T. Neupert, C.-K. Chiu, S.-M. Huang, G. Chang, I. Belopolski, D. S. Sanchez, M. Neupane, N. Alidoust, C. Liu, B. Wang, C.-C. Lee, H.-T. Jeng, A. Bansil, F. Chou, H. Lin, and M. Zahid Hasan, “Topological nodal-line fermions in spin-orbit metal  $PbTaSe_2$ ,” *Nature Communications* **7**, 10556 (2016).
- [63] Lilia S. Xie, Leslie M. Schoop, Elizabeth M. Seibel, Quinn D. Gibson, Weiwei Xie, and Robert J. Cava, “A new form of  $Ca_3P_2$  with a ring of dirac nodes,” *APL Mater.* **3**, 083602 (2015).
- [64] Jun-Won Rhim and Yong Baek Kim, “Landau level quantization and almost flat modes in three-dimensional semimetals with nodal ring spectra,” *Phys. Rev. B* **92**, 045126 (2015).
- [65] Y. Chen, Y. Xie, S. A. Yang, H. Pan, F. Zhang, M. L. Cohen, and S. Zhang, “Spin-orbit-free Weyl-loop and Weyl-point semimetals in a stable three-dimensional carbon allotrope,” ArXiv e-prints (2015), arXiv:1505.02284 [cond-mat.mtrl-sci].
- [66] Chen Fang, Yige Chen, Hae-Young Kee, and Liang Fu, “Topological nodal line semimetals with and without spin-orbital coupling,” *Phys. Rev. B* **92**, 081201 (2015).
- [67] Guang Bian, Tay-Rong Chang, Hao Zheng, Saavanth Velury, Su-Yang Xu, Titus Neupert, Ching-Kai Chiu, Shin-Ming Huang, Daniel S. Sanchez, Ilya Belopolski, Nasser Alidoust, Peng-Jen Chen, Guoqing Chang, Arun Bansil, Horng-Tay Jeng, Hsin Lin, and M. Zahid Hasan, “Drumhead surface states and topological nodal-line fermions in  $tl_2Te_2$ ,” *Phys. Rev. B* **93**, 121113 (2016).
- [68] Rui Yu, Zhong Fang, Xi Dai, and Hongming Weng, “Topological nodal line semimetals predicted from first-principles calculations,” *Frontiers of Physics* **12**, 127202 (2017).
- [69] J.-W. Rhim and Y. B. Kim, “Anisotropic density fluctuations, plasmons, and Friedel oscillations in nodal line semimetal,” *New Journal of Physics* **18**, 043010 (2016), arXiv:1511.07885 [cond-mat.str-el].
- [70] Zhongbo Yan, Peng-Wei Huang, and Zhong Wang, “Collective modes in nodal line semimetals,” *Phys. Rev. B* **93**, 085138 (2016).
- [71] Lih-King Lim and Roderich Moessner, “Pseudospin vortex ring with a nodal line in three dimensions,” *Phys. Rev. Lett.* **118**, 016401 (2017).
- [72] C. Fang, H. Weng, X. Dai, and Z. Fang, “Topological nodal line semimetals,” *Chinese Physics B* **25**, 117106 (2016),

- arXiv:1609.05414 [cond-mat.mes-hall].
- [73] Jianpeng Liu and Leon Balents, “Correlation effects and quantum oscillations in topological nodal-loop semimetals,” *Phys. Rev. B* **95**, 075426 (2017).
- [74] J. L. Lu, W. Luo, X. Y. Li, S. Q. Yang, J. X. Cao, X. G. Gong, and H. J. Xiang, “Two-Dimensional Node-Line Semimetals in a Honeycomb-Kagome Lattice,” *ArXiv e-prints* (2016), arXiv:1603.04596 [cond-mat.mtrl-sci].
- [75] Y.-H. Chan, Ching-Kai Chiu, M. Y. Chou, and Andreas P. Schnyder, “ $ca_3p_2$  and other topological semimetals with line nodes and drumhead surface states,” *Phys. Rev. B* **93**, 205132 (2016).
- [76] Qiunan Xu, Rui Yu, Zhong Fang, Xi Dai, and Hongming Weng, “Topological nodal line semimetals in the  $ca_3$  family of materials,” *Phys. Rev. B* **95**, 045136 (2017).
- [77] Ronghan Li, Hui Ma, Xiyue Cheng, Shoulong Wang, Dianzhong Li, Zhengyu Zhang, Yiyi Li, and Xing-Qiu Chen, “Dirac node lines in pure alkali earth metals,” *Phys. Rev. Lett.* **117**, 096401 (2016).
- [78] Motoaki Hirayama, Ryo Okugawa, Takashi Miyake, and Shuichi Murakami, “Topological dirac nodal lines and surface charges in fcc alkaline earth metals,” *Nature Communications* **8**, 14022 (2017).
- [79] Jin Hu, Zhijie Tang, Jinyu Liu, Xue Liu, Yanglin Zhu, David Graf, Yanmeng Shi, Shi Che, Chun Ning Lau, Jiang Wei, *et al.*, “Topological nodal-line fermions in zrsise and zrsite,” *arXiv preprint arXiv:1604.06860* (2016).
- [80] Leslie M Schoop, Mazhar N Ali, Carola Straßer, Viola Duppel, Stuart SP Parkin, Bettina V Lotsch, and Christian R Ast, “Dirac cone protected by non-symmorphic symmetry and 3d dirac line node in zrsis,” *arXiv preprint arXiv:1509.00861* (2015).
- [81] R. Singha, A. Pariari, B. Satpati, and P. Mandal, “Titanic magnetoresistance and signature of non-degenerate Dirac nodes in ZrSiS,” *ArXiv e-prints* (2016), arXiv:1602.01993 [cond-mat.mtrl-sci].
- [82] Madhab Neupane, Ilya Belopolski, M. Mofazzel Hosen, Daniel S. Sanchez, Raman Sankar, Maria Szlowska, Su-Yang Xu, Klauss Dimitri, Nagendra Dhakal, Pablo Maldonado, Peter M. Oppeneer, Dariusz Kaczorowski, Fangcheng Chou, M. Zahid Hasan, and Tomasz Durakiewicz, “Observation of topological nodal fermion semimetal phase in zrsis,” *Phys. Rev. B* **93**, 201104 (2016).
- [83] X. Wang, X. Pan, M. Gao, J. Yu, J. Jiang, J. Zhang, H. Zuo, M. Zhang, Z. Wei, W. Niu, Z. Xia, X. Wan, Y. Chen, F. Song, Y. Xu, B. Wang, G. Wang, and R. Zhang, “Evidence of both surface and bulk Dirac bands in ZrSiS and the unconventional magnetoresistance,” *ArXiv e-prints* (2016), arXiv:1604.00108 [cond-mat.mtrl-sci].
- [84] C Chen, X Xu, J Jiang, S-C Wu, YP Qi, LX Yang, MX Wang, Y Sun, NBM Schröter, HF Yang, *et al.*, “Dirac line nodes and effect of spin-orbit coupling in the nonsymmorphic critical semimetals msis ( $m=hf, zr$ ),” *Physical Review B* **95**, 125126 (2017).
- [85] Zhongbo Yan and Zhong Wang, “Tunable weyl points in periodically driven nodal line semimetals,” *Phys. Rev. Lett.* **117**, 087402 (2016).
- [86] Ching-Kit Chan, Yun-Tak Oh, Jung Hoon Han, and Patrick A. Lee, “Type-ii weyl cone transitions in driven semimetals,” *Phys. Rev. B* **94**, 121106 (2016).
- [87] Awadhesh Narayan, “Tunable point nodes from line-node semimetals via application of light,” *Phys. Rev. B* **94**, 041409 (2016).
- [88] X.-X. Zhang, T. Tzen Ong, and N. Nagaosa, “Theory of photoinduced Floquet Weyl semimetal phases,” *ArXiv e-prints* (2016), arXiv:1607.05941 [cond-mat.mtrl-sci].
- [89] Katsuhisa Taguchi, Dong-Hui Xu, Ai Yamakage, and K. T. Law, “Photovoltaic anomalous hall effect in line-node semimetals,” *Phys. Rev. B* **94**, 155206 (2016).
- [90] Y. Du, F. Tang, D. Wang, L. Sheng, E.-j. Kan, C.-G. Duan, S. Y. Savrasov, and X. Wan, “CaTe: a new topological node-line and Dirac semimetal,” *ArXiv e-prints* (2016), arXiv:1605.07998 [cond-mat.mtrl-sci].
- [91] S. Kobayashi, Y. Yamakawa, A. Yamakage, T. Inohara, Y. Okamoto, and Y. Tanaka, “Crossing-Line-Node Semimetals: General Theory and Application to Rare-Earth Trihydrides,” *ArXiv e-prints* (2017), arXiv:1703.03587 [cond-mat.mes-hall].
- [92] T. Bzdušek, Q. Wu, A. Rüegg, M. Sigrist, and A. A. Soluyanov, “Nodal-chain metals,” *Nature (London)* **538**, 75–78 (2016), arXiv:1604.03112 [cond-mat.mes-hall].
- [93] R. Yu, Q. Wu, Z. Fang, and H. Weng, “From Nodal Chain Semimetal To Weyl Semimetal in HfC,” *ArXiv e-prints* (2017), arXiv:1701.08502 [cond-mat.mtrl-sci].
- [94] Y. X. Zhao and Y. Lu, “Pt-symmetric real dirac fermions and semimetals,” *Phys. Rev. Lett.* **118**, 056401 (2017).
- [95] Frank Wilczek and A. Zee, “Linking numbers, spin, and statistics of solitons,” *Phys. Rev. Lett.* **51**, 2250–2252 (1983).
- [96] Mikio Nakahara, *Geometry, topology and physics* (CRC Press, 2003).
- [97] Eduardo Fradkin, *Field theories of condensed matter physics* (Cambridge University Press, 2013).
- [98] Joel E Moore, Ying Ran, and Xiao-Gang Wen, “Topological surface states in three-dimensional magnetic insulators,” *Physical review letters* **101**, 186805 (2008).
- [99] D.-L. Deng, S.-T. Wang, C. Shen, and L.-M. Duan, “Hopf insulators and their topologically protected surface states,” *Phys. Rev. B* **88**, 201105 (2013).
- [100] D.-L. Deng, S.-T. Wang, K. Sun, and L.-M. Duan, “Probe knots and Hopf insulators with ultracold atoms,” *ArXiv e-prints* (2016), arXiv:1612.01518 [cond-mat.mes-hall].
- [101] D.-L. Deng, S.-T. Wang, and L.-M. Duan, “Systematic construction of tight-binding hamiltonians for topological insulators and superconductors,” *Phys. Rev. B* **89**, 075126 (2014).
- [102] Ricardo Kennedy, “Topological hopf-chern insulators and the hopf superconductor,” *Phys. Rev. B* **94**, 035137 (2016).
- [103] Chunxiao Liu, Farzan Vafa, and Cenke Xu, “Symmetry-protected topological hopf insulator and its generalizations,” *Phys. Rev. B* **95**, 161116 (2017).
- [104] Paul J. Ackerman and Ivan I. Smalyukh, “Diversity of knot solitons in liquid crystals manifested by linking of preimages in torons and hopfions,” *Phys. Rev. X* **7**, 011006 (2017).
- [105] C. Wang, P. Zhang, X. Chen, J. Yu, and H. Zhai, “Measuring Topological Number of a Chern-Insulator from Quench Dynamics,” *ArXiv e-prints* (2016), arXiv:1611.03304 [cond-mat.quant-gas].
- [106] Zhongbo Yan, Ren Bi, and Zhong Wang, “Majorana zero modes protected by a hopf invariant in topologically trivial superconductors,” *Phys. Rev. Lett.* **118**, 147003 (2017).
- [107] Shinsei Ryu and Yasuhiro Hatsugai, “Topological origin of zero-energy edge states in particle-hole symmetric systems,” *Phys. Rev. Lett.* **89**, 077002 (2002).
- [108] Note that  $\Pi_x, \Pi_y$  do not commute. We take the symmetric ordering for operators, e.g.,  $k_x k_y^2 \rightarrow (\Pi_x \Pi_y \Pi_y + \Pi_y \Pi_x \Pi_y + \Pi_y \Pi_y \Pi_x)/3$ .
- [109] G. P. Mikitik and Yu. V. Sharlai, “Manifestation of berry’s phase in metal physics,”

- Phys. Rev. Lett. **82**, 2147–2150 (1999).
- [110] L. Onsager, “Interpretation of the de Haas-van Alphen effect,” The London, Edinburgh, and Dublin Philosophical Magazine and Journal of Science **43**, 1006–1008 (1952).
- [111] Di Xiao, Ming-Che Chang, and Qian Niu, “Berry phase effects on electronic properties,” Rev. Mod. Phys. **82**, 1959–2007 (2010).
- [112] Netanel H Lindner, Gil Refael, and Victor Galitski, “Floquet topological insulator in semiconductor quantum wells,” Nature Physics **7**, 490–495 (2011).
- [113] Takuya Kitagawa, Takashi Oka, Arne Brataas, Liang Fu, and Eugene Demler, “Transport properties of nonequilibrium systems under the application of light: Photoinduced quantum hall insulators without Landau levels,” Phys. Rev. B **84**, 235108 (2011).
- [114] Takashi Oka and Hideo Aoki, “Photovoltaic hall effect in graphene,” Phys. Rev. B **79**, 081406 (2009).
- [115] Jun-ichi Inoue and Akihiro Tanaka, “Photoinduced transition between conventional and topological insulators in two-dimensional electronic systems,” Phys. Rev. Lett. **105**, 017401 (2010).
- [116] Zhenghao Gu, H. A. Fertig, Daniel P. Arovas, and Assa Auerbach, “Floquet spectrum and transport through an irradiated graphene ribbon,” Phys. Rev. Lett. **107**, 216601 (2011).
- [117] Takuya Kitagawa, Mark S. Rudner, Erez Berg, and Eugene Demler, “Exploring topological phases with quantum walks,” Phys. Rev. A **82**, 033429 (2010).
- [118] Takuya Kitagawa, Erez Berg, Mark Rudner, and Eugene Demler, “Topological characterization of periodically driven quantum systems,” Phys. Rev. B **82**, 235114 (2010).
- [119] Liang Jiang, Takuya Kitagawa, Jason Alicea, A. R. Akhmerov, David Pekker, Gil Refael, J. Ignacio Cirac, Eugene Demler, Mikhail D. Lukin, and Peter Zoller, “Majorana fermions in equilibrium and in driven cold-atom quantum wires,” Phys. Rev. Lett. **106**, 220402 (2011).
- [120] Mark S. Rudner, Netanel H. Lindner, Erez Berg, and Michael Levin, “Anomalous edge states and the bulk-edge correspondence for periodically driven two-dimensional systems,” Phys. Rev. X **3**, 031005 (2013).
- [121] Biao Lian, Cumrun Vafa, Farzan Vafa, and Shou-Cheng Zhang, “Chern-Simons theory and Wilson loops in the Brillouin zone,” Phys. Rev. B **95**, 094512 (2017).
- [122] Wei Chen, Hai-Zhou Lu, and Jing-Min Hou, “Topological semimetals with a double-helix nodal link,” arXiv preprint arXiv:1703.10886 (2017).
- [123] M. Ezawa, “Topological Semimetals carrying Arbitrary Hopf Numbers: Hopf-Link, Solomon’s-Knot, Trefoil-Knot and Other Semimetals,” ArXiv e-prints (2017), arXiv:1704.04941 [cond-mat.mes-hall].

## Supplemental Material

### HAMILTONIAN IN REAL SPACE

The Hamiltonians studied in the main article have been written down in the momentum space. In this supplemental material we provide their explicit expressions in real space.

For the Hamiltonian with  $a_1 = d_x(\mathbf{k})$  and  $a_3 = d_z(\mathbf{k})$  (abbreviated as  $d_x$ - $d_z$  Hamiltonian), the tight-banding form in real space is

$$\begin{aligned}
 H = \sum_{lmn} \{ & [m_0(c_{l,m,n}^\dagger \tau_z c_{l+1,m,n} + c_{l,m,n}^\dagger \tau_z c_{l,m+1,n} + c_{l,m,n}^\dagger \tau_z c_{l,m,n+1}) + h.c.] - \frac{1}{2}(c_{l,m,n}^\dagger \tau_z c_{l+2,m,n} + c_{l,m,n}^\dagger \tau_z c_{l,m+2,n} + h.c.) \\
 & - \frac{1}{2}(c_{l,m,n}^\dagger \tau_z c_{l+1,m+1,n} + c_{l,m,n}^\dagger \tau_z c_{l+1,m-1,n} + c_{l,m,n}^\dagger \tau_z c_{l+1,m,n+1} + c_{l,m,n}^\dagger \tau_z c_{l+1,m,n-1} + c_{l,m,n}^\dagger \tau_z c_{l,m+1,n+1} + c_{l,m,n}^\dagger \tau_z c_{l,m+1,n-1} + h.c.) \\
 & - (m_0^2 + 1)c_{l,m,n}^\dagger \tau_z c_{l,m,n} + m_0(c_{l,m,n}^\dagger i\tau_x c_{l,m+1,n} + h.c.) - \frac{1}{2}(c_{l,m,n}^\dagger i\tau_x c_{l,m+2,n} + h.c.) + \frac{1}{2}(c_{l,m,n}^\dagger \tau_x c_{l+1,m,n-1} - c_{l,m,n}^\dagger \tau_x c_{l+1,m,n+1} + h.c.) \\
 & + \frac{1}{2}(c_{l,m,n}^\dagger i\tau_x c_{l+1,m-1,n} - c_{l,m,n}^\dagger i\tau_x c_{l+1,m+1,n} + c_{l,m,n}^\dagger i\tau_x c_{l,m-1,n+1} - c_{l,m,n}^\dagger i\tau_x c_{l,m+1,n+1} + h.c.) \}, \quad (16)
 \end{aligned}$$

where  $\{l, m, n\}$  labels the lattice sites along the  $\{x, y, z\}$  axis, respectively;  $c_{l,m,n} = (c_{l,m,n;a}, c_{l,m,n;b})^T$ , where  $a$  and  $b$  denote

two degrees of freedom.

For the  $d_x$ - $d_y$  Hamiltonian, the tight-banding form in the real space is

$$\begin{aligned}
 H = \sum_{lmn} \{ & m_0(c_{l,m,n}^\dagger i\tau_x c_{l,m+1,n} + c_{l,m,n}^\dagger i\tau_y c_{l+1,m,n} + h.c.) - \frac{1}{2}(c_{l,m,n}^\dagger i\tau_x c_{l,m+2,n} + c_{l,m,n}^\dagger i\tau_y c_{l+2,m,n} + h.c.) \\
 & + \frac{1}{2}(c_{l,m,n}^\dagger \tau_x c_{l+1,m,n-1} - c_{l,m,n}^\dagger \tau_x c_{l+1,m,n+1} + c_{l,m,n}^\dagger \tau_y c_{l,m+1,n+1} - c_{l,m,n}^\dagger \tau_y c_{l,m+1,n-1} + h.c.) \\
 & + \frac{1}{2}(c_{l,m,n}^\dagger i\tau_x c_{l+1,m-1,n} - c_{l,m,n}^\dagger i\tau_x c_{l+1,m+1,n} + c_{l,m,n}^\dagger i\tau_x c_{l,m-1,n+1} - c_{l,m,n}^\dagger i\tau_x c_{l,m+1,n+1} + h.c.) \\
 & - \frac{1}{2}(c_{l,m,n}^\dagger i\tau_y c_{l+1,m+1,n} + c_{l,m,n}^\dagger i\tau_y c_{l+1,m-1,n} + c_{l,m,n}^\dagger i\tau_y c_{l+1,m,n+1} + c_{l,m,n}^\dagger i\tau_y c_{l+1,m,n-1} + h.c.) \}. \quad (17)
 \end{aligned}$$

## SEMICLASSICAL DERIVATION OF LANDAU LEVELS IN A MAGNETIC FIELD

The semiclassical quantization condition in a magnetic field along the  $z$  direction is [109–111] ( $\hbar = c = 1$ )

$$S(k_z) = 2\pi eB(n + \gamma), \quad (18)$$

where  $S$  denotes the cross-sectional area of the orbital in momentum space,  $n$  is a positive integer, and  $\gamma$  is a constant given by

$$\gamma = \frac{1}{2} - \frac{\phi_B}{2\pi}. \quad (19)$$

Here,  $\phi_B$  is the Berry phase:

$$\phi_B = \oint_{\partial S} \mathbf{a} \cdot d\mathbf{k}, \quad (20)$$

where  $\partial S$  denotes the boundary of  $S$ , and  $\mathbf{a}$  is the Berry connection of the valence band.

The energy spectra of the  $d_x$ - $d_y$  model  $H(\mathbf{k}) = 2[k_x k_z + (m - Ck^2)k_y]\tau_x + 2[-k_y k_z + (m - Ck^2)k_x]\tau_y$  are

$$E_{\pm}(\mathbf{k}) = \pm 2 \sqrt{(k_x^2 + k_y^2)[k_z^2 + (m - Ck^2)^2]}. \quad (21)$$

Because of the rotational symmetry, the  $\mathbf{k}$ -space orbital in the presence of magnetic field along the  $z$  direction is a circle in the  $k_x$ - $k_y$  plane, in other words, the  $\mathbf{k}$ -space cross-sectional area  $S$  of the semiclassical motion is given by

$$S = \pi(k_x^2 + k_y^2). \quad (22)$$

As a result, the energy spectra can be rewritten as

$$E_{\pm}(\mathbf{k}) = \pm 2 \sqrt{\frac{S}{\pi}[k_z^2 + (m - Ck_z^2 - C\frac{S}{\pi})^2]}. \quad (23)$$

For the  $d_x$ - $d_y$  Hamiltonian in consideration, there is a toroidal Berry phase  $\phi_B = \pi$ , therefore,  $\gamma = 0$ , and we have, according to Eq.(18):

$$S = 2\pi eBn. \quad (24)$$

Inserting this relation into Eq.(23), we immediately obtain the Landau levels in terms of  $B$ :

$$E_{n,\pm}(k_z) = \pm \sqrt{8neB[k_z^2 + (m - Ck_z^2 - 2nCeB)^2]}, \quad n \geq 1 \quad (25)$$

which is consistent with the exact quantum mechanical solutions.

For the single-nodal-ring model  $H(\mathbf{k}) = (m - Ck^2)\tau_x + k_z\tau_z$ , the toroidal Berry phase  $\phi_B = 0$ , thus we have  $\gamma = 1/2$ , and

$$S = 2\pi eB(n + 1/2) \quad (26)$$

according to Eq.(18). The energy spectra of the Hamiltonian are

$$\begin{aligned} E_{\pm}(\mathbf{k}) &= \pm \sqrt{k_z^2 + (m - Ck^2)^2} \\ &= \pm \sqrt{k_z^2 + (m - Ck_z^2 - C\frac{S}{\pi})^2}, \end{aligned} \quad (27)$$

where  $S = \pi(k_x^2 + k_y^2)$  has been used. With the formula of  $S$  inserted, the Landau levels take the form of

$$E_{n,\pm}(k_z) = \pm \sqrt{k_z^2 + [m - Ck_z^2 - 2(n + \frac{1}{2})CeB]^2}, \quad (28)$$

which is again consistent with the exact quantum-mechanical solutions. Notice the difference between  $n$  and  $n + 1/2$  in the Eq.(25) and Eq.(28). This semiclassical derivation shows that this difference comes from the toroidal Berry phase, which is  $\pi$  for a linked ring and 0 for an unlinked ring.

## SURFACE STATES OF FLOQUET HOPF INSULATORS

In the main article, we have obtained an effective time-independent Hamiltonian in the off-resonance regime:

$$\begin{aligned} H_{\text{eff}}(\mathbf{k}) &= \mathcal{H}_0 + \sum_{n \geq 1} \frac{[\mathcal{H}_n, \mathcal{H}_{-n}]}{n\omega} + O\left(\frac{1}{\omega^2}\right) \\ &= 2[k_x k_z + k_y(\tilde{m}_2 - Ck^2)]\tau_x + 2[-k_y k_z + k_x(\tilde{m}_2 - Ck^2)]\tau_y \\ &\quad + \lambda[k_z^2 + (\tilde{m}_1 - Ck^2)^2 - 2Ck_\rho^2(\tilde{m}_1 - Ck^2 - \frac{\gamma}{4})]\tau_z, \end{aligned} \quad (29)$$

where  $\lambda \equiv 4\eta e^2 A_0^2 / \omega$ ,  $\gamma \equiv C e^2 A_0^2$  and  $k_\rho = \sqrt{k_x^2 + k_y^2}$ . It is readily found that the energy spectrum of  $H_{\text{eff}}$  is fully gapped.

To see how the surface state evolves under the periodic driving, we treat the photo-induced  $\tau_z$  term as a perturbation and consider that the system occupies the  $z > 0$  region. Without the  $\tau_z$  term, the energy dispersion of the surface state can be obtained by solving the eigenvalue equation  $H_{\text{eff}}(k_x, k_y, -i\partial_z)\Psi_{k_x, k_y}(z) = E(k_x, k_y)\Psi_{k_x, k_y}(z)$  under the boundary condition  $\Psi_{k_x, k_y}(0) = \Psi_{k_x, k_y}(+\infty) = 0$ . A straightforward calculation gives

$$\Psi_{k_x, k_y}(z) = \mathcal{N} e^{ik_x x + ik_y y} e^{-\kappa_1 z} \sin(\kappa_2 z) \begin{pmatrix} 0 \\ 1 \end{pmatrix}, \quad (30)$$

where  $\kappa_1 = 1/2C$ ,  $\kappa_2 = \sqrt{4C(\tilde{m}_2 - Ck_\rho^2) - 1/2C}$ , and  $\mathcal{N}$  is a normalization factor. The normalizability requires  $\tilde{m}_2 > Ck_\rho^2$ , which determines the region within which surface states exist. Without the  $\tau_z$  term, we find that the surface state dispersion is  $E(k_x, k_y) = 0$ , in other words, the energy spectrum of the surface state is completely flat without the periodic driving. Now we add the photo-induced  $\tau_z$  term. Based on the first-order perturbation theory, we find

$$\begin{aligned} \Delta E(k_x, k_y) &= \int_0^{+\infty} dz \Psi_{k_x, k_y}^*(z) d_{\text{eff}, z}(k_x, k_y, -i\partial_z) \tau_z \Psi_{k_x, k_y}(z) \\ &= -\lambda[\tilde{m}_2/C + \gamma^2 - (1 + 3C\gamma/2)k_\rho^2]. \end{aligned} \quad (31)$$

If the system occupies the  $z < 0$  region instead of the  $z > 0$  region, similar procedures lead to similar dispersion as Eq.(31), except that the sign is reversed. Thus, for a finite but sufficiently thick sample, the energy dispersion for the surface states localized at the surfaces is

$$E_\alpha(\mathbf{k}) = \alpha\lambda[\tilde{m}_2/C + \gamma^2 - (1 + 3C\gamma/2)k_\rho^2], \quad (32)$$

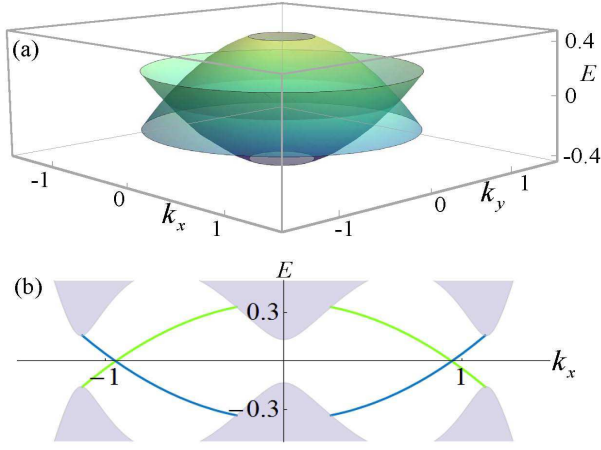


FIG. 4. Energy dispersion of the surface states of a slab of Floquet Hopf insulator (with a pseudo-magnetic field  $\Delta\tau_z$  added). Parameters are  $\omega = 4$ ,  $m = 1$ ,  $eA_0 = 0.6$ ,  $C = 0.5$ ,  $\Delta = -0.3\lambda$  with  $\lambda = 4(eA_0)^2/\omega$ . (a) 3D view. (b)  $E(k_x)$  with  $k_y = 0$  fixed. The grey regions represent the bulk bands.

where  $\alpha = + (-)$  for top (bottom) surface. As shown in Fig.3, the two energy bands of the surface state will cross at certain  $k_\rho$ , forming a nodal ring in the two dimensional momentum space, which is characteristic of a Hopf insulator.

As briefly mentioned in the main article, the size of the gap is of the order of  $(eA_0)^4$ , which is generally quite small under realistic experimental conditions. This shortcoming can be overcome by introducing a pseudo-magnetic field  $\Delta\tau_z$  into  $H_{\text{eff}}$  (At this stage, this  $\Delta\tau_z$  term is added phenomenologically. Its physical realization depends on specific system in consideration). As long as  $|\Delta| < |\lambda|\tilde{m}_1^2$  and  $\eta\Delta < 0$ , the driven Hamiltonian remains in the nontrivial Hopf insulating phase, but with the gap modified to  $\tilde{E}_g = \min\{2\Delta + E_g, 2(|\lambda|\tilde{m}_1^2 - \Delta)\}$ , which is of the order of  $(eA_0)^2$ . Moreover, the energy dispersion of the surface states is modified to

$$\tilde{E}_\alpha(\mathbf{k}) = \alpha \left( \lambda[\tilde{m}_2/C + \gamma^2 - (1 + 3C\gamma/2)k_\rho^2] + \Delta \right), \quad (33)$$

which is shown in Fig.4.

### FLOQUET HOPF INSULATOR FROM NODAL-LINK SEMIMETAL: THE LATTICE MODEL.

In the main article, we have studied the effect of periodic driving to the linked nodal rings based on a continuum model. We have obtained a Floquet Hopf insulator. To further corroborate this conclusion, we include here the results for a lattice model.

The lattice Hamiltonian is

$$H(\mathbf{k}) = 2[\sin k_x \sin k_z + \sin k_y \left( \sum_i \cos k_i - m_0 \right)]\tau_x + 2[-\sin k_y \sin k_z + \sin k_x \left( \sum_i \cos k_i - m_0 \right)]\tau_y, \quad (34)$$

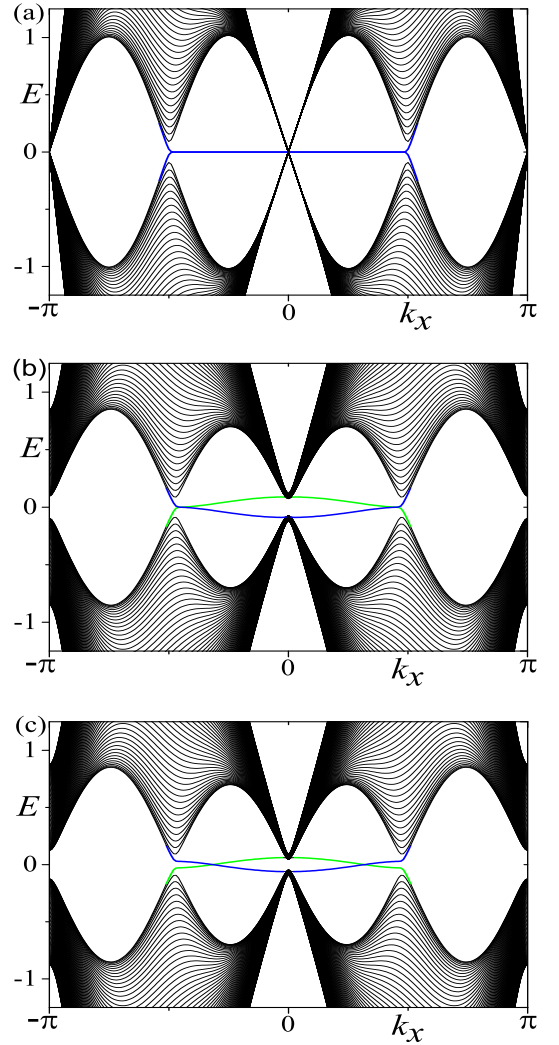


FIG. 5. Surface states evolution of a slab sample under periodic driving. The thickness of slab is 100 site.  $k_y = 0$  is fixed. Common parameters:  $m_0 = 2$ . (a) The static case. The surface state is of the characteristic “drumhead” form. (b)  $eA_0 = 0.5$ ,  $\omega = 10$  and  $\eta = 1$ . The green and blue lines denote surface states on the top and bottom surface, respectively. (c) The parameters are the same as in (b), except that a pseudo-magnetic field term  $\Delta\tau_z$  is added, with  $\Delta = -0.3\lambda$ .

whose continuum limit is studied in the main article. With the introduction of a circularly polarized light (CPL) propagating in  $z$  direction, the effect of periodic driving is described by  $H(\mathbf{k}) \rightarrow H[\mathbf{k} + e\mathbf{A}(t)]$  with  $\mathbf{A}(t) = A_0(\cos \omega t, \eta \sin \omega t, 0)$  with  $\eta = \pm 1$  denoting the two kinds of helicity of CPL. As the full Hamiltonian is time-periodic,  $H(\mathbf{k}, t + T) = H(\mathbf{k}, t)$  with  $T = 2\pi/\omega$ , it can be expanded as  $H(\mathbf{k}, t) = \sum_n \mathcal{H}_n(\mathbf{k}) e^{in\omega t}$ . By applying the identities for Bessel function,  $\exp[x(\xi - \xi^{-1})/2] = \sum_{n=-\infty}^{\infty} J_n(x)\xi^n$ ,  $J_{-n}(x) = (-1)^n J_n(x)$ , and  $J_n(-x) =$

$(-1)^n J_n(x)$ , we find

$$\begin{aligned}\sin(k_x + eA_0 \cos \omega t) &= \sum_{n=-\infty}^{\infty} J_n(eA_0) i^n e^{in\omega t} [-ie^{ik_x} + (-1)^n ie^{-ik_x}] / 2, \\ \sin(k_y + eA_0 \eta \sin \omega t) &= \sum_{n=-\infty}^{\infty} J_n(eA_0) e^{in\omega t} \eta^n [-ie^{ik_y} + (-1)^n ie^{-ik_y}] / 2, \\ \cos(k_x + eA_0 \cos \omega t) &= \sum_{n=-\infty}^{\infty} J_n(eA_0) i^n e^{in\omega t} [e^{ik_x} + (-1)^n e^{-ik_x}] / 2, \\ \cos(k_y + eA_0 \eta \sin \omega t) &= \sum_{n=-\infty}^{\infty} J_n(eA_0) e^{in\omega t} \eta^n [e^{ik_y} + (-1)^n e^{-ik_y}] / 2.\end{aligned}$$

It is straightforward to find that

$$\begin{aligned}\mathcal{H}_n(\mathbf{k}) &= \left\{ J_n(eA_0) i^n [-ie^{ik_x} + (-1)^n ie^{-ik_x}] \sin k_z \right. \\ &\quad + J_n(eA_0) \eta^n [-ie^{ik_y} + (-1)^n ie^{-ik_y}] (\cos k_z - m_0) \\ &\quad + \sum_{l=-\infty}^{\infty} J_l(eA_0) J_{n-l} i^{n-l} \eta^l [-ie^{ik_y} + i(-1)^l e^{-ik_y}] \\ &\quad \times [e^{ik_x} + (-1)^{n-l} e^{-ik_x}] / 2 + \sum_{l=-\infty}^{\infty} [J_l(eA_0) J_{n-l}(eA_0) \eta^n \\ &\quad \times [-ie^{ik_y} + i(-1)^l e^{-ik_y}] [e^{ik_x} + (-1)^{n-l} e^{-ik_x}] / 2 \left. \right\} \tau_x \\ &\quad + \left\{ J_n(eA_0) \eta^n [ie^{ik_y} - (-1)^n ie^{-ik_y}] \sin k_z \right. \\ &\quad + J_n(eA_0) i^n [-ie^{ik_x} + (-1)^n ie^{-ik_x}] (\cos k_z - m_0) \\ &\quad + \sum_{l=-\infty}^{\infty} J_l(eA_0) J_{n-l}(eA_0) i^n [-ie^{ik_x} + i(-1)^l e^{-ik_x}] \\ &\quad \times [e^{ik_x} + (-1)^{n-l} e^{-ik_x}] / 2 + \sum_{l=-\infty}^{\infty} J_l(eA_0) J_{n-l}(eA_0) i^l \eta^{n-l} \\ &\quad \times [-ie^{ik_x} + i(-1)^l e^{-ik_x}] [e^{ik_y} + (-1)^{n-l} e^{-ik_y}] / 2 \left. \right\} \tau_y.\end{aligned}\quad (36)$$

We focus on the regime  $eA_0 < 1$  in which  $J_{|n|}(eA_0)$  decrease rapidly with the increasing of  $|n|$ , so that it is justified to keep only  $\mathcal{H}_0$  and  $\mathcal{H}_{\pm 1}$ , and ignore terms containing  $J_n(eA_0)$  with  $|n| \geq 2$ . The explicit form of  $\mathcal{H}_0$  and  $\mathcal{H}_{\pm 1}$  are

$$\begin{aligned}\mathcal{H}_0(\mathbf{k}) &= \left\{ 2J_0(eA_0) [\sin k_x \sin k_z + \sin k_y (\cos k_z - m_0)] + 2J_0^2(eA_0) \sin k_y \cos k_x + 2[J_0^2(eA_0) - 2J_1^2(eA_0)] \sin k_y \cos k_y \right\} \tau_x \\ &\quad + \left\{ 2J_0(eA_0) [-\sin k_y \sin k_z + \sin k_x (\cos k_z - m_0)] + 2[J_0^2(eA_0) - 2J_1^2(eA_0)] \sin k_x \cos k_x + 2J_0^2(eA_0) \sin k_x \cos k_y \right\} \tau_y \\ \mathcal{H}_{+1}(\mathbf{k}) &= \left\{ 2J_1(eA_0) [\cos k_x \sin k_z - i\eta \cos k_y (\cos k_z - m_0)] - 2iJ_0(eA_0) J_1(eA_0) (\eta \cos k_x \cos k_y - i \sin k_x \sin k_y) \right. \\ &\quad \left. - 2i\eta J_0(eA_0) J_1(eA_0) \cos 2k_y \right\} \tau_x + \left\{ 2J_1(eA_0) [i\eta \cos k_y \sin k_z + \cos k_x (\cos k_z - m_0)] \right. \\ &\quad \left. + 2J_0(eA_0) J_1(eA_0) \cos 2k_x + 2J_0(eA_0) J_1(eA_0) (\cos k_x \cos k_y + i\eta \sin k_x \sin k_y) \right\} \tau_y, \\ \mathcal{H}_{-1}(\mathbf{k}) &= \left\{ 2J_1(eA_0) [\cos k_x \sin k_z + i\eta \cos k_y (\cos k_z - m_0)] + 2iJ_0(eA_0) J_1(eA_0) (\eta \cos k_x \cos k_y + i \sin k_x \sin k_y) \right. \\ &\quad \left. + 2i\eta J_0(eA_0) J_1(eA_0) \cos 2k_y \right\} \tau_x + \left\{ 2J_1(eA_0) [-i\eta \cos k_y \sin k_z + \cos k_x (\cos k_z - m_0)] \right. \\ &\quad \left. + 2J_0(eA_0) J_1(eA_0) \cos 2k_x + 2J_0(eA_0) J_1(eA_0) (\cos k_x \cos k_y - i\eta \sin k_x \sin k_y) \right\} \tau_y.\end{aligned}\quad (37)$$

We consider the off-resonant regime, in which the effective

time-independent Hamiltonian is given by

$$\begin{aligned}H_{\text{eff}}(\mathbf{k}) &= \mathcal{H}_0 + \frac{[\mathcal{H}_{+1}, \mathcal{H}_{-1}]}{\omega} + O\left(\frac{1}{\omega^2}\right) \\ &= \left\{ 2J_0(eA_0) [\sin k_x \sin k_z + \sin k_y (\cos k_z - m_0)] + 2J_0^2(eA_0) \sin k_y \cos k_x + 2[J_0^2(eA_0) - 2J_1^2(eA_0)] \sin k_y \cos k_y \right\} \tau_x \\ &\quad + \left\{ 2J_0(eA_0) [-\sin k_y \sin k_z + \sin k_x (\cos k_z - m_0)] + 2[J_0^2(eA_0) - 2J_1^2(eA_0)] \sin k_x \cos k_x + 2J_0^2(eA_0) \sin k_x \cos k_y \right\} \tau_y \\ &\quad + \lambda \left\{ \cos k_x \cos k_y [(\cos k_z - m_0)^2 + \sin^2 k_z] + J_0(eA_0) (\cos 2k_x \cos k_y + \cos k_x \cos 2k_y + \cos^2 k_x \cos k_y + \cos k_x \cos^2 k_y) \right. \\ &\quad \times (\cos k_z - m_0) + J_0(eA_0) (\cos k_x - \cos k_y) \sin k_x \sin k_y \sin k_z \\ &\quad \left. + J_0^2(eA_0) [\cos 2k_x \cos 2k_y + \cos k_x \cos k_y (\cos 2k_x + \cos 2k_y) + \cos^2 k_x \cos^2 k_y - \sin^2 k_x \sin^2 k_y] \right\} \tau_z,\end{aligned}\quad (38)$$

where  $\lambda = 16\eta J_1^2(eA_0)/\omega$ .

Now we study the surface states. We consider a slab perpendicular to the  $z$  direction, with periodic boundary condition in the  $x$  and  $y$  directions. The numerical results are shown in Fig.5. Without periodic driving, the energy dispersion of the surface state is found to be completely flat, as shown in Fig.5(a). In the presence of periodic driving, the surface state becomes dispersive. Besides, the two energy bands of the surface states (from top and bottom surfaces) are found to cross

each other along a closed line, which is a characteristic property of Hopf insulators. After adding a pseudo-magnetic field  $\Delta\tau_z$  to  $H_{\text{eff}}$  (note that such a constant term does not affect the form of the photo-induced part of the effective Hamiltonian), the crossing of the two surface energy bands becomes more prominent, as shown in Fig.5(c). It is apparent that the above results for the lattice model qualitatively agrees with that of the continuum model.